Journal of Sound and Vibration (1998) **215**(2), 211–229
Article No. sv971665

A SMART INTERNAL VIBRATION SUPPRESSOR FOR A HELICOPTER BLADE— A FEASIBILITY STUDY

J. P. NARKIEWICZ

Institute of Aeronautics and Applied Mechanics, Warsaw University of Technology, ul. Nowowiejska 24, *Warsaw, Poland*

AND

G. T. S. DONE

Department of Mechanical Engineering and Aeronautics, School of Engineering, City University, Northampton Square, London EC1V 0HB, England

(*Received* 8 *November* 1996, *and in final form* 9 *October* 1997)

The concept of a vibration suppression device mounted inside the rotor blade of a helicopter is evaluated. Two problems are considered. First, the possibility of reducing the vibration level by applying generic/non-specific dynamic loads is examined. An optimisation technique is used to provide the most effective parameters of the applied loads. It is shown possible to obtain a reduction in vibration level by applying dynamic loads along the part of the blade span. Next the concept of using an active "bender" type element for vibration suppression mounted inside the blade and attached to the blade main spar is studied. The bender is modelled as an elastic cantilever beam sandwiched on the longitudinal faces normal to the bending plane by layers of piezoelectric material. When an alternating voltage is applied to the piezoelectric layers, the element is excited into a bending motion, which leads to a dynamic force and moment reaction at the attachment point. The performance of such a device is studied using a computer model of a hingeless rotor blade. The bender placement and design parameters are varied in order to obtain insight into their influence on the vibration suppression. For currently practical blade and bender parameters considered it appears that excitation by the blade motion overrides the control available from the piezoelectric device, although future developments in piezoelectric material performance will improve the situation.

1. INTRODUCTION

The components on which helicopter performance and handling qualities depend most crucially are the main and tail rotors. Improvement of these elements leads to an enhancement of the overall rotorcraft quality. This provides the motivation for many investigations into the possibilities of smart structure applications in rotorcraft.

Recently, several different concepts of smart rotors have been investigated [1]. From the design point of view these are tuning the dynamic properties of the rotor, adapting the blade shape to the ambient flight, and operating some additional device mounted on the blades.

0022–460X/98/320211 + 19 $30.00/0

Shape adaptive blades can be constructed to change the blade twist, the shape of the blade cross-section, and the deflection in and out of the plane of rotation. Application of shape adapting blades directly to full scale rotors appears to be not currently possible because of insufficient actuating power and questions of reliability of existing smart materials.

The loads on rotor blades can also be influenced by using leading or trailing edge control surfaces. The use of blade trailing edge tabs for primary control has been successfully implemented by Kaman in their products, most recently on the K-Max helicopter.

In the design of a trailing edge tab actuated by smart materials, different driving mechanisms are concerned as the key factor. In some proposed solutions [2–4] a piezoelectric bender was used for controlling the tab. Tabs driven by piezoelectric benders were tested experimentally in reference [4] on a rotor model in hover.

It seems to be a very promising concept, so several analytical studies have been carried out to obtain insight into different aspects of the application of a trailing edge tab. The use of tabs for primary control was investigated in reference [5], for vibration suppression in reference [6], for blade vortex interaction reduction in reference [7] and for rotor performance optimisation in reference [8].

Physical phenomena involved in "smart tab" applications are both aerodynamic and dynamic i.e., involving inertia and elastic loads. Up till now only the effect of aerodynamic influence on rotor behaviour has been investigated, the influence of blade motion on the actuating device having not yet been considered.

The aim of this study is to explore the possibility of reducing the blade vibration level by dynamic activity only, avoiding interference with the aerodynamic environment, i.e., involving only inertial and elastic forces. The anti-vibration device is designed as a smart element mounted inside the blade.

The topics considered in this study are: (1) the incorporation of a smart bender into the blade model; (2) the possibility of suppressing blade vibration by applying only dynamic loads; (3) the exploration of the behaviour of the blade and a blade mounted vibration suppressor.

First, the possibility of reducing the vibration level by applying non-specific dynamic loads at a selected part of the blade radius is explored using an optimisation technique for parametric study. An index of vibration level is based on loads at the blade root in a rotating frame of reference. This part of the research allows evaluation of the possibility of eliminating different vibration components by dynamic activity.

In the second part of the study, the coupled motion of blade and internally mounted bender is explored to reveal the possibility of direct application of this kind of device. The possibility of influencing the motion of the bender by actuating smart layers is studied. This investigation provides a basis for use in designing bender type driving mechanisms for actuating trailing edge tabs.

2. ROTOR BLADE MODEL

The computer model of an individual rotor blade, developed in reference [9] for investigation of the influence of various hub and blade designs on rotor behaviour, was used in this study. It allows the modelling of an articulated, hingeless and bearingless rotor by different arrangements of hub hinges and deflections of the blade. The most general case with all hinges and blade deflections is described briefly for completeness, bearing in mind that any subcase is provided by changing control parameters in the computer code.

A helicopter rotor in steady flight is considered. The angular velocity Ω of the rotor shaft is constant.

2.1. HUB CONFIGURATION

A blade attachment to the rotor shaft can be composed in many different ways including from none to three hinges in arbitrary sequence.

The most general hub model shown in Figure 1 consists of four stiff segments described by vectors **e**, **f**, **g**, **h**. These segments link the blade to the rotor shaft. Length and orientation of the segments relative to the shaft allow for different hinge placement within the hub.

At the end of each segment a flap, lag or pitch hinge can be placed, the angles being modelled by rotation transformation matrices.

Coupling between rotations of the hub hinges (such as kinematic pitch–flap coupling resulting from geometry of the pitch arm) can also be taken into account, in addition to any coupling effect resulting from the placement of the hub segments.

2.2. BLADE

The blade is attached to the hub at the point A at the end of the segment **h**. The blade can be rigid or deformable. It is treated as a slender body, having arbitrary planform along the span, and geometrically twisted about the straight axis of the last hub segment in the rigid case, or about its elastic axis if the blade is deformable.

In this study the blade is modelled as a beam.

2.3. GENERALISED CO-ORDINATES

The blade motion is comprised of rotations at the hub hinges $\beta_i(t)$ and deflections, namely, in-plane bending $v(x, t)$, out-of-plane bending $w(x, t)$ and torsion $\phi(x, t)$. The blade deformations are discretized by free vibration, rotating modes:

$$v(x, t) = \sum_{i=1}^{N_v} \eta_i(x) q_i(t) \qquad w(x, t) = \sum_{i=N_v+1}^{N_v+N_w} \eta_i(x) q_i(t)$$

$$\phi(x, t) = \sum_{i=N_v+N_w+1}^{N_v+N_w+N_f} \eta_i(x) q_i(t).$$

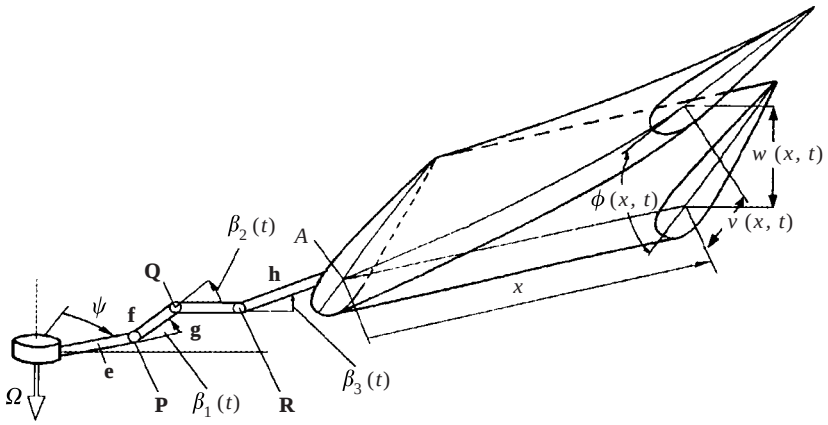

Figure 1. General model of the blade.

For each type of blade deformation i.e. lag, flap, and twist the number of modes are assumed to be N_v, N_w, N_f, respectively.

The vector of generalised co-ordinates of blade motion consists of: elastic degrees of freedom resulting from discretisation of blade deformations; rigid degrees of freedom corresponding to the rotations at the hinges.

$$\mathbf{p} = \{p_i\} = \{p_j, \beta_i\}, \qquad j = 1, \ldots, N_v + N_w + N_f, \qquad i = 0/1/2/3, \qquad p_i(t, x) = \eta_i(x) q_i(t).$$

Each generalised co-ordinate can be a sum of: constant parts $\mathbf{p}_0$, which correspond to configurational parameters such as precone, droop, etc., angles or blade curvature; periodic components $\mathbf{p}_t(t)$, which describe the steady blade motion; unknown functions $\mathbf{q}(t)$, which describe a disturbed blade motion

$$\mathbf{p}(t) = \mathbf{p}_0 + \mathbf{p}_t(t) + \mathbf{q}(t).$$

Blade pitch control angle $\theta(t)$ is added to the pitch hinge rotation θ, if appropriate. Blade pitch control is assumed in the form:

$$\theta(t) = \theta_0 + \theta_1 \cos(\Omega t) + \theta_2 \sin(\Omega t).$$

If there are both pitch and flap hinges in the hub, kinematic pitch–flap coupling can be applied.

2.4. EQUATIONS OF MOTION

The equations of motion are defined using Hamilton's Principle, which leads to equations in Lagrangian form. The inertia, elastic, aerodynamic and damping loads have separate and distinct derivations within the equations, and are described in more detail below.

2.4.1. *Inertia loads*

The kinetic energy of an elemental mass on a blade is formulated initially by establishing its instantaneous position in space relative to fixed axes. This involves introducing the various translation and rotation transformation matrices necessary to transform a position vector expressed relative to the undeformed blade, to one relative to fixed axes. The total kinetic energy is formed by integration, and application of Lagrange's equations leads to the inertia loads in the following matrix form:

$$IL = \mathbf{B}(\mathbf{q})\ddot{\mathbf{q}} + 2\mathbf{C}(\mathbf{q})\dot{\mathbf{q}} + \mathbf{g}_m(\dot{\mathbf{q}}, \mathbf{q}) + \mathbf{f}_m(\mathbf{q}).$$

The elements of the matrices $\mathbf{B}$, $\mathbf{C}$, and the vectors $\mathbf{g}_m$, $\mathbf{f}_m$ are given in Appendix A.

2.4.2. *Elastic loads*

The general expression for elastic loads has the form:

$$\mathbf{Q}_E = \mathbf{Q}_E(\mathbf{q}).$$

It is composed of expressions describing elastic loads in hinges and those of the deflected blade.

The elastic loads in the hinges are prescribed non-linear functions of rotations

$$EL_H = \mathbf{Q}_H(\mathbf{q}).$$

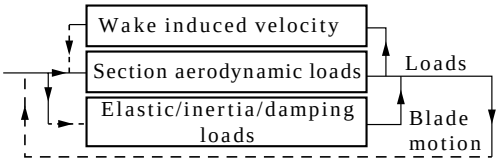

Figure 2. The flow decomposition for a two-dimensional model.

If a deformable blade, it is considered to twist about a longitudinal axis and bend in two perpendicular directions. In this study, blade elastic loads are derived from the model given in reference [10].

The base assumptions are that the undeformed blade has a straight elastic axis, the blade cross-sections have symmetry of elastic properties about the chord, and after deformation there is neither cross-section distortion nor section warping. The deflections are considered small and the curvature moderate.

After discretisation using rotating natural modes, the stiffness load expression for elastic degrees of freedom in the equations of motion can be put in the form:

$$EL_E = \mathbf{Aq} + \mathbf{h}.$$

The elements of matrix **A** and the vector **h** are given in Appendix B.

2.4.3. *Aerodynamic loads*

The aerodynamic loads are calculated by strip theory using a two-dimensional model. The flow (Figure 2) is decomposed into an internal part, where the aerodynamic loads on the aerofoil section are calculated and an external part manifesting itself as induced velocity generated by rotor wake.

The aerodynamic loads on a section at the aerodynamic centre AC (Figure 3) are:

drag:

$$\mathrm{d}D = \tfrac{1}{2}\rho c(x)V^2(x)C_D(\alpha)\,\mathrm{d}x,$$

lift:

$$\mathrm{d}L = \tfrac{1}{2}\rho c(x)V^2(x)C_L(\alpha)\,\mathrm{d}x,$$

moment:

$$\mathrm{d}M = \tfrac{1}{2}\rho c^2(x)V^2(x)C_M(\alpha)\,\mathrm{d}x,$$

where ρ is the air density and $c(x)$ is the section chord.

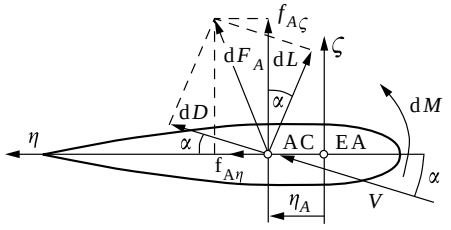

Figure 3. Aerodynamic loads on a blade section.

The flow velocity vector **V** results from the velocity of helicopter flight, blade motion relative to a helicopter fuselage including shaft rotation, angles at the hinges and deformation and induced velocity $\mathbf{v}_i$. The component of air flow velocity relative to the helicopter can be allowed to vary with time, which enables the inclusion of the analysis of gusts.

The section angle of attack a is calculated using the components of vector **V**

$$\alpha = a \tan\left(\frac{V_\zeta}{V_\eta}\right).$$

The aerofoil aerodynamic coefficients for drag $C_D(\alpha)$, lift $C_L(\alpha)$ and moment $C_M(\alpha)$ are obtained for a section at instantaneous angles of attack α by a table look-up procedure, which allows for non-linear characteristics.

The induced velocity $\mathbf{v}_i$ is calculated from the Glauert formula [11].

The vector of rotor aerodynamic loads can be written as a non-linear operator in a general form

$$\mathbf{Q}_A = \mathbf{Q}_A(t, \dot{\mathbf{q}}, \mathbf{q}).$$

The components of this vector needed in the equations of motion are obtained via successive transformation to the appropriate co-ordinate systems. They are rotated into a section of a deformed blade first, and then into a system of co-ordinates in a section of the blade before deformation. The generalised aerodynamic forces for the elastic degrees of freedom are obtained in this system by multiplying by appropriate deflection modes and integrating along the span.

Aerodynamic loads are transformed to the root of the blade and integrated along the blade length. The components of these loads are taken into the appropriate equations of motion for the rigid body degrees of freedom, these components being made zero in the subsequent transformation.

The total blade aerodynamic loads at the shaft axis, multiplied by the number of blades are taken into the inflow model.

2.4.4. *Damping loads*

Non-linear damping and/or stiffness can be included as arbitrary functions of hinge rotation angles and angular velocities. For blade deflections viscous damping loads are assumed. In the equations of motion, damping is expressed as non-linear vector $\mathbf{Q}_D(\dot{\mathbf{q}}, \mathbf{q})$.

2.4.5. *Final form of blade equations of motion*

Collecting together the expressions, the equations of motion are put in the form:

$$\mathbf{B}(\mathbf{q})\ddot{\mathbf{q}} = -2\mathbf{C}(\mathbf{q})\dot{\mathbf{q}} - \mathbf{g}(\dot{\mathbf{q}}, \mathbf{q}) - \mathbf{f}(\mathbf{q}) + \mathbf{Q}_A(t, \dot{\mathbf{q}}, \mathbf{q}) + \mathbf{Q}_D(\dot{\mathbf{q}}, \mathbf{q}) - \mathbf{Q}_E(\mathbf{q}).$$

To avoid numerical difficulties the derivatives of matrices and vectors needed for formulating these equations are obtained analytically and included in the computer code, where they are arranged according to the chosen hub model. Algebraic manipulations for obtaining coefficients in the equations of motion are performed within the computer program.

The blade generalised masses and stiffnesses are calculated within a separate routine that is run only once for the assumed blade configuration before solving (or analysing) the equations of motion. Thus, the inertia and structural loads need not be integrated along the blade span during the computation of the right hand sides of the equations.

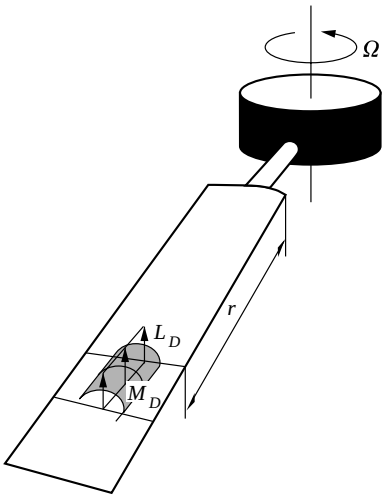

Figure 4. Control load distribution along the blade.

2.5. BLADE MOTION ANALYSIS

The first step of the analysis is to define the blade model i.e., the number and sequence of hub hinges and number of modes for blade deflections.

The equations of motion are included in a set of computer codes designed to perform a comprehensive stability analysis. For the case with no parametric excitation, the steady deformations are obtained from the set of non-linear algebraic equations with velocities and accelerations excluded. The numerical integration of the equations of motion is performed using Gear's algorithm. To calculate a blade steady motion, the equations are integrated numerically for a prescribed number of rotor revolutions and the steady motion taken to be that given by the values achieved during the final rotation.

3. EVALUATION OF A CAPABILITY TO SUPPRESS VIBRATION

3.1. METHODOLOGY

This section of the paper is aimed at assessing the possibility of reducing vibration levels by applying pure dynamic loads along the part of blade span.

The influence of the vibration suppression device on the blade is modelled as a normal force and twisting moment distributed locally over part of the blade span (Figure 4). The values of these loads, called controlled or additional loads, are varied in such a way as to diminish the blade vibrations.

A blade vibration level is quantified by indices J_{Fk}, $(k = 1, 2, \ldots, 6)$ which are calculated individually for any k-th component of the blade load (force and moment) at the prescribed place on the blade

$$J_{Fk} = \frac{\sum_{i=1}^{M} |F_{k0}(\psi_i) - F_k(\psi_i)|}{\sum_{i=1}^{M} |F_{k0}(\psi_i)|},$$

where $F_{k0}(\psi_i)$ is the base ("required") value of the blade load, $F_k(\psi_i)$ is the actual value of the blade load, and M is the number of azimuth stations for one rotation. These indices are calculated for blade steady motion during one rotor rotation and reflect the relation of the difference of the base and actual values of a load to the required load.

The values of the base blade loads $F_{k0}(\psi_i)$ needed for indices calculations can be determined from consideration of the overall helicopter trim, or they can arise from the need to reduce a particular blade load component and/or one of its harmonics.

To evaluate the improvement in vibration suppression, the relative performance indices are calculated according to the formula

$$\Delta J_{Fk} = \frac{J_{Fk0} - J_{Fk}}{J_{Fk0}},$$

where J_{Fk0} is the index value before suppression activity, and J_{Fk} is the index value after suppression activity.

The vibration reduction depends on flight conditions and design parameters of both the blade and the vibration suppressor. To assess the possibility of reducing the overall vibration level, a parametric study is performed. To avoid excessive computations during such a study an optimisation procedure is utilised to obtain the most suitable sets of chosen parameters of controlled loads.

The method selected is the Powell algorithm, described in reference [12]. This is a non-gradient method, using the concept of a penalty function with self-adjusting direction and step size to search for the minimum of the quality index. This algorithm forms a part of the computations to minimise a performance index for a prescribed blade load component.

An optimisation constraint in these calculations arises by assuming that the rotor thrust coefficient must not vary more than a prescribed fraction of the basic value. Imposing this constraint is necessary in order to prevent minimising the vibration level to zero by application of very high controlled loads.

After selecting the blade model and the required blade loads and expressions for controlled loads, the sequence of steps leading to application of this methodology is as follows. (1) Assume the blade model and helicopter flight conditions. (2) Select the blade base loads $F_{k0}(\psi_i)$. (3) Calculate the rotor thrust coefficient to constrain the optimisation process. (4) Calculate the starting value of the vibration indices J_{Fk0} (for the blade without additional loads). (5) Select the expressions for controlled loads and optimisation parameters in these expressions. (6) Use the optimisation algorithm to obtain the values of parameters minimising the selected vibration index. (7) Calculate the final value of vibration indices J_{Fk} and improvement in vibration level ΔJ_{Fk}.

3.2. IMPLEMENTATION AND RESULTS OF CALCULATIONS

The base blade configuration selected for this study comprises the deformable blade attached to the shaft via a stiff element having lag offset. The blade can be controlled in pitch about a feathering bearing.

Numerical results are obtained using a Westland Lynx blade [13] for the base data, given in Table 1.

The flight conditions concern an untrimmed rotor with collective pitch control of 13° and no cyclic control. The flow velocity is expressed as a rotor advance ratio which varies from 0 to 0·35 in 0·05 intervals. The controlled loads are distributed on part of the blade starting from blade section $0{\cdot}83R$ along a short length of span of 0·2 m i.e., $0{\cdot}032R$. This vibration index is measured at a blade root.

The controlled loads are dependent on time (azimuth) in the general form of harmonic excitation.

$$M_D = \sum_{n=0}^{N} A_{Dn} \cos(n\psi + \varphi_{0n}) \qquad L_D = \sum_{n=0}^{N} B_{Dn} \cos(n\psi + \varphi_{0n}).$$

The loads on the pitch controlled, non-deflecting blade are taken as the required loads. This simulates the most stringent requirements for vibration reduction, since at the blade root the only loads needed are those actually required for achieving the appropriate flight condition.

The blade loads are calculated for blade steady motion which is obtained by numerical integration of the equations of motion for the prescribed number of rotor revolutions.

The optimisation variables in the order of use inside the algorithm are amplitudes, frequencies and phase angles of the loads respectively. The sets of these parameters differ according to the case considered, as described below. Within the algorithm the order of searching for values which minimise blade loads is first by applying the moment, then force, then frequency change, and finally phase angle. This order corresponds to static optimisation first, followed by dynamic i.e., changing forces in time.

A typical plot, Figure 5, shows the changes in relative performance index based on forces and moments at the blade root. The curves plotted illustrate minimisation using the optimisation algorithm of single load components at the blade root.

The separate curves in these figures are not individually identified because it is the general trend of the curves collectively which is important for the subsequent considerations. The results of three groups of computations, Cases I, II and III, are presented below. Details of these are given in Table 2.

Case I

The controlled loads with only one harmonic are considered. The same frequency and phase angle is assumed for the additional moment and force. This assumption reflects the fact that prospective common sources of these loads result from the same inertia forces. Optimising parameters are amplitudes of force and moment, the frequency and phase.

TABLE 1

Blade base data

Quantity	Value	Units
Rotor radius	6·40	m
Blade length	5·61	m
Blade chord	0·395	m
Lead-lag offset	0·025	m
Blade mass	57·16	kg
Flap mass static moment	121·61	kg m
Flap inertia moment	437·54	kg m^2
Angular velocity	34·17	rad/s
Air density	1·225	kg/m^3
Linear twist: at the root	4·3°	
at the tip	−2·2°	
Deformation	Freq. 1/rev	Damping %
Lag	0·656	1
Flap	1·087	3
Twist	6·298	1

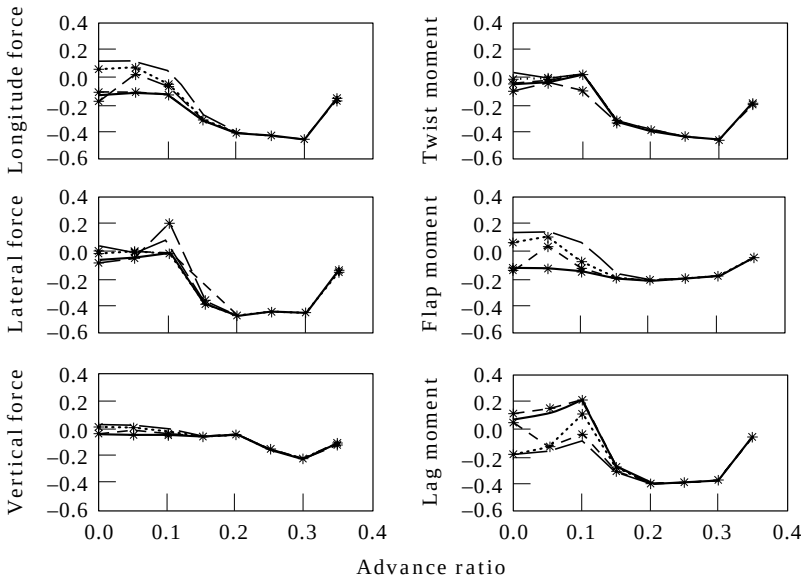

Figure 5. Change of performance index by optimising selected components for fully elastic blade.

The improvement in vibration indices obtained for the base blade model are presented in Figure 5 and the amplitudes of the optimal controlled loads in Figure 6. The amplitudes of moment and force are non-dimensionalised by dividing by $0{\cdot}5\rho U_T^2 c(x)^2$ and $0{\cdot}5\rho U_T^2 c(x)$, respectively.

It can be concluded that minimisation of one component of blade load also usually implies minimisation of all other load components. In some cases, even when the optimisation is unsuccessful for an assumed blade load, the minimisation of other components occurs.

TABLE 2

Cases analysed

Case no.	Blade degrees of freedom	Additional loads	Optimisation variables	Figure no.
I	Flap, lag and twist, one mode for each deflection	$M_D = A_{Dn}\cos(n\psi + \varphi_{0n})$ $L_D = B_{Dn}\cos(n\psi + \varphi_{0n})$	A_{Dn}, B_{Dn}, n, φ_{n0}	5, 6
I	Flap bending, rigid pitch	as above	as above	7
I	Twist	as above	as above	8
II	Flap, lag and twist, one mode for each deflection	$M_D = A_{Dn}\cos(n\psi + \varphi_{0n})$ $L_D = B_{Dn}\cos(n\psi + \varphi_{0n})$ $n = 1, 2, 3, 4, 5$	A_{Dn}, B_{Dn}, φ_{v0}	9
III	Flap, lag and twist, one mode for each deflection	$M_D = \sum_{n=1}^{4} A_{Dn}\cos(n\psi + \varphi_{0n})$ $L_D = KM_D$	A_{Dn}, B_{Dn}, φ_{v0}	10

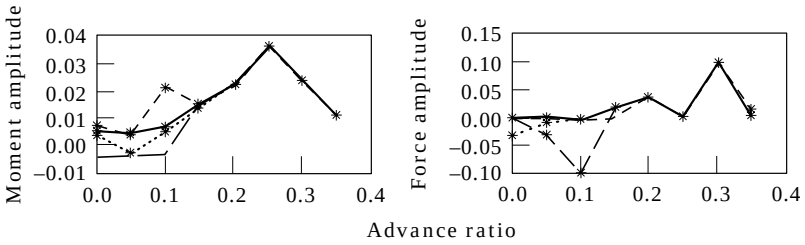

Figure 6. Amplitudes of the applied force and moment for the vibration indices in Figure 5.

Some difficulties with vibration suppression at low-speed flight are apparent. For cruise flight an improvement in vibration level up to 40% of the base level can be achieved.

In the case considered, the optimisation algorithm produced no significant frequency or phase changes.

Two other blade models are also considered. The first has as blade degrees of freedom rigid rotation at the pitch bearing and flapwise bending deflection, the second only blade torsion. These arrangements can be considered to be models of special types of blades, in which selected deflections are suppressed. Figures 7 and 8 show the changes in resultant blade root vertical force and twisting moment; the results seem to be not so consistent, and in some cases the minimisation of the vibration index has been unsuccessful.

Resulting from this part of the study, the normal force and twisting moment at the blade root are chosen from all components of blade loads for Cases II and III to follow, these being the components of blade load most directly influenced by the controlled load.

Case II

In this case, loads at the blade root are minimised assuming constant exciting frequency for the additional force and moment. Frequencies 1, 2, 3, 4, 5 per rev are considered. The results of the vibration index calculation for the vertical forces and twisting moments are shown in Figure 9.

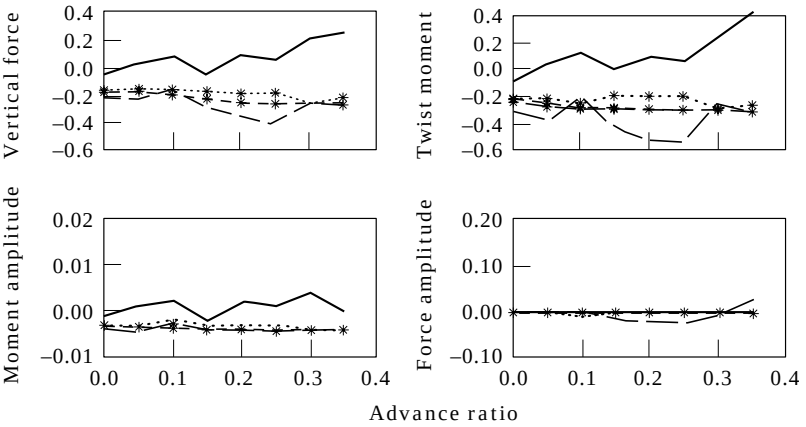

Figure 7. Change of vibration index for the blade deformable flap-wise and rotating in pitch bearing.

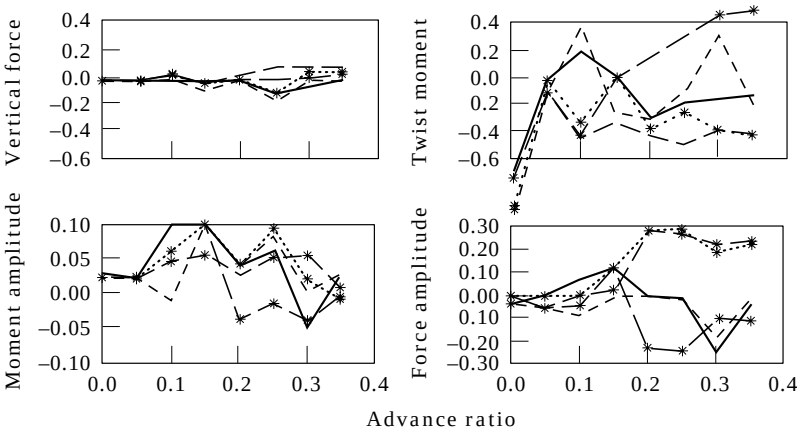

Figure 8. Change in vibration index for the blade deformable in twist only.

For all cases, the computed phase angles are inconsistent, which suggests that the optimisation algorithm does not behave well in dynamic analysis. When the vibration index is based on twisting moment (all the curves with the longer dashed lines) vibration suppression is more effective for all load components. The application of the first and fifth harmonic does not seem to be efficient, compared with the 2, 3, and 4 per rev. The best results are obtained for excitations of 2 and 3 per rev, and the 4 per rev gives the smoothest function.

Case III

In the last case in this group of computations the controlled loads are in the form

$$M_D = \sum_{n=1}^{4} A_{Dn} \cos(n\psi + \varphi_n), \qquad L_D = KM_D.$$

These formulae reflect the fact that, in the case of the dynamic suppressor, the common source of loads is inertia force. For a definite design of bender the relationship of inertia moment to inertia force is fixed. For the case of the bender considered in the next section of this paper $K = 3{\cdot}0$. The optimisation parameters are the amplitudes and the phases of four harmonics of controlled loads. The indices based on vertical force and twisting moment are shown in Figure 10 for minimising each load at the blade root.

In this case, minimising the vertical force leads to an increase in vibration for twisting moment. The overall level of vibration suppression is less than in the previous cases.

The final conclusions which can be drawn from the three cases above are as follows: (1) There is a potential for reducing the varying loads at the blade root by applying only dynamic loads along part of the blade span. (2) These loads can be adjusted to minimise a selected component at the blade root. (3) The results of the minimisation depend on the blade model considered, which implies that each blade configuration should be analysed individually. (4) It is possible for the minimisation of one component of blade load to lead to a reduction in vibration level of the other components.

The final conclusion provides a useful indication in the design of control algorithms based on blade force measurement. The methodology developed above provides a tool for selecting an appropriate load component to use in a sensor application.

4. BLADE WITH DYNAMIC BENDER TYPE DEVICE

The aim of this part of the study is to explore the behaviour of a rotor blade with an embedded, actively controlled, bender type device. The base blade arrangement is used here.

4.1. BENDER MODEL

The active element comprises a "bender", i.e., an elastic beam element, attached to the blade main spar, mounted inside the external envelope of the aerofoil (Figure 11). It is sandwiched on the longitudinal faces normal to the beam bending plane by layers of smart material. When an alternating voltage is applied to the layers, the element is excited into a bending motion, which leads to a dynamic force and moment reaction at the attachment

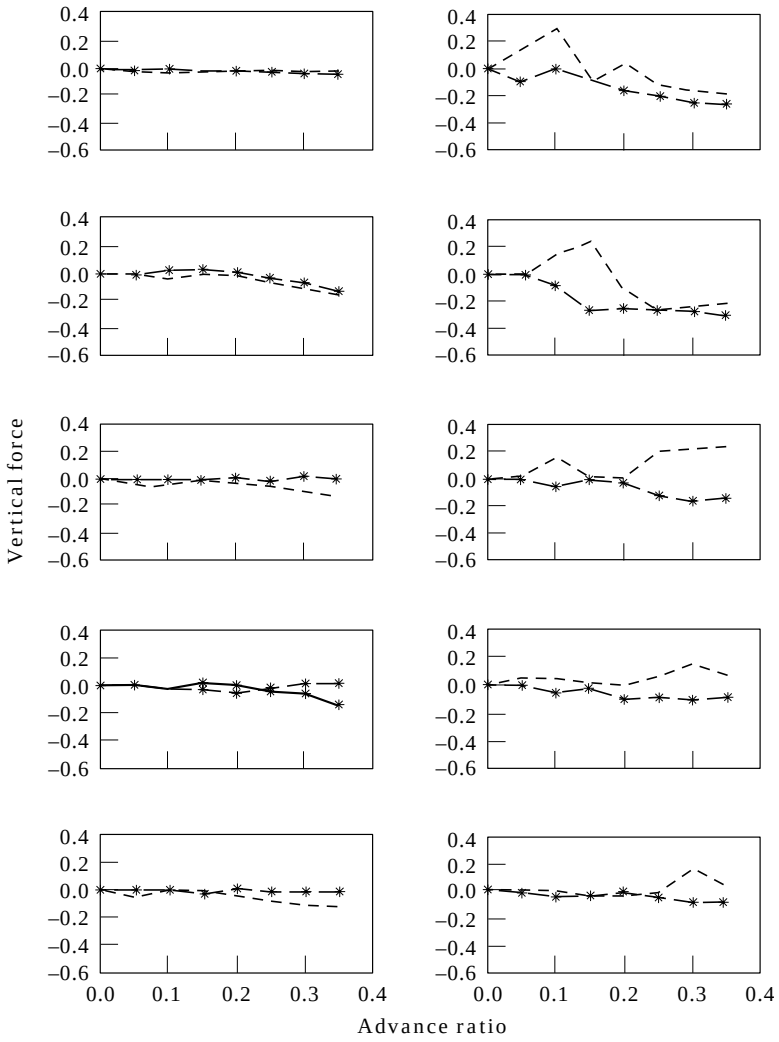

Figure 9. Change in performance index for excitation by selected harmonics 1, 2, 3, 4, 5 per rev (reading down the page). Base model.

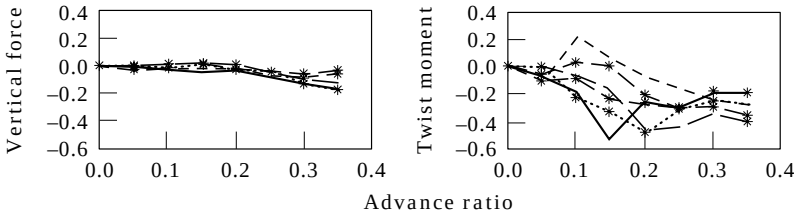

Figure 10. Change in vibration index for "dynamic type" loads. Base model.

point. To operate effectively, the dynamic loads at its root should produce an adequate force and twisting moment about the elastic axis of the blade.

The assumptions used in the bender computer model are: (1) The bender is a cantilevered Euler–Bernoulli beam. (2) The materials of beam and smart layers are isotropic and uniform. (3) The upper and lower surfaces of the beam are covered by a layer of smart material. (4) Viscous damping for each bending mode is assumed. The Lagrange equations of motions are derived and the normal mode equations are obtained by the Galerkin method.

The external load, resulting from beam/layer interaction is calculated using the model described in reference [14] for the piezoelectric layers. The external bending moments from the piezoelectric layers equations of motion are:

$$M_l = 2\eta_{lT} b d_{31} E_p (t_b + t_l) t_b U(t),$$

where b is the width of the bender, d_{31} is the piezoelectric constant, E_p is the modulus of elasticity of piezoelectric, t_b is the thickness of the beam, t_l is the thickness of the layer, $U(t)$ is the voltage applied, η_{iT} is the angle of deflection at the end of the bender for the ith mode.

This model stems from consideration of a cantilever beam with two thin layers of active materials bonded symmetrically on both sides of the neutral axis. The thickness of the bonding material ("glue") is assumed negligible and connection of piezoelectrics and beam is assumed perfect.

The base bender data in this case are given in Table 3.

4.2. BLADE–BENDER INTERACTION

Blade motion is studied for the following cases: (A) Blade without bender. (B) Bender mounted inside the blade, excited by the blade motion, with blade deflections unaffected by bender motion. (C) Coupled motion of blade with bender. (D) Coupled motion of blade with bender excited by harmonic voltage.

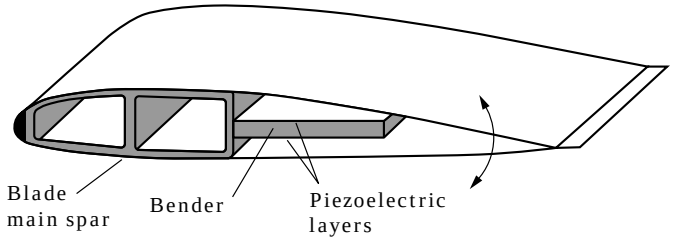

Figure 11. The bender type vibration suppressor mounted inside the blade.

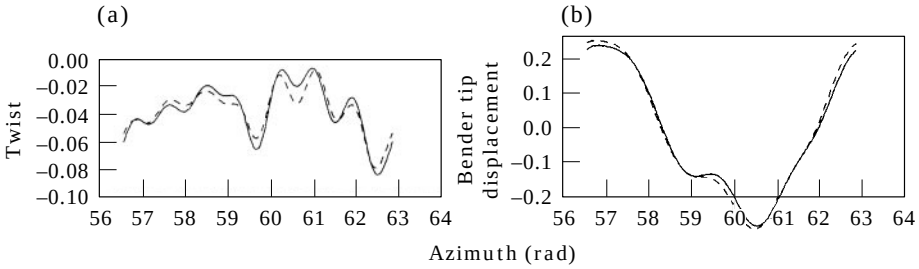

Figure 12. Influence of bender/blade dynamic coupling. (a) – – –, No bender; ——, with bender. (b) – – –, No coupling; — · —, coupled.

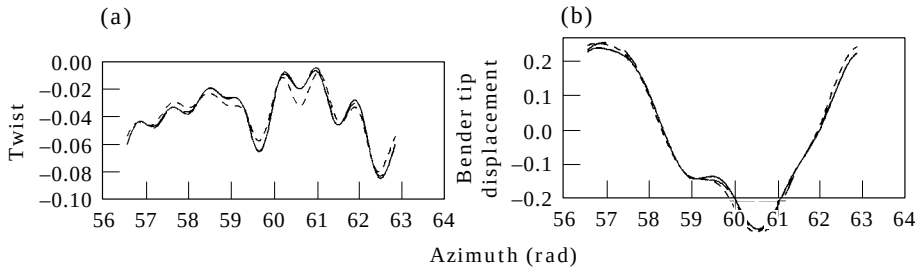

Figure 13. Influence of bender/blade dynamic coupling on possibility of excitation of bender motion: – – –, no bender; ——, with bender; — · —, with bender 1/rev.

The results of computations are presented for the last rotor rotation of the series of rotations assumed for calculation of blade steady motion (i.e., after nine revolutions). Twist angles are given in radians, tip displacements in metres.

Comparing the blade motion for cases A and B (without and with bender mounted at radius $0{\cdot}83R$) no influence on blade flap and lag motion is observed. The influence of embedding the bender on blade twist angle and the bender tip motion for this case is shown in Figure 12. The deflections of the bender tip are unrealistically high, due to excitation from blade motion.

The attempt to influence the bender motion by exciting the piezoelectric layers harmonically at 1 per rev with a voltage amplitude 200 V are shown in Figure 13 for blade

TABLE 3

Bender data

Quantity	Units	Beam	Layer
Material		steel	PZT
Young's modulus	N/m^2	$21{\cdot}6 \times 10^{10}$	$6{\cdot}2 \times 10^{10}$
Density	kg/m^3	7800	7600
Piezoelectric coefficient d_{13}	V/m		$1{\cdot}9 \times 10^{10}$
Height	m	0·01	0·0005
Length	m	0·25	0·25
Width	m	0·2 (3·1%R)	Full surface covered
Number of modes		1	
Mode shape		Cantilevered beam	
Damping	% crit	0·5	

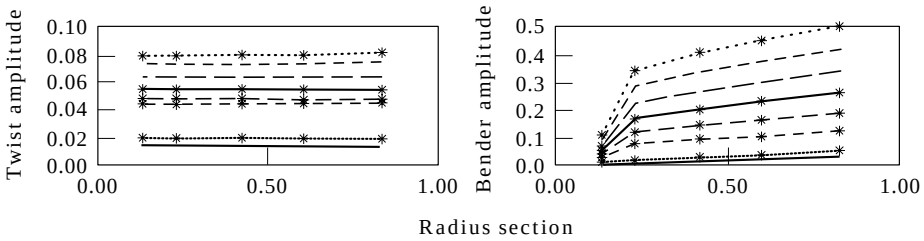

Figure 14. Influence of bender radial placement on amplitudes of blade twist and bender tip displacement: ——, $\mu = 0{\cdot}00$; ---∗---, $\mu = 0{\cdot}05$; –∗–, $\mu = 0{\cdot}10$; —∗—, $\mu = 0{\cdot}15$; —∗—, $\mu = 0{\cdot}20$; — —, $\mu = 0{\cdot}25$; – – –, $\mu = 0{\cdot}30$; ---∗---, $\mu = 0{\cdot}35$.

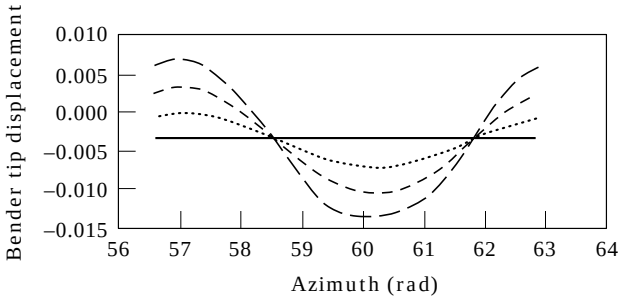

Figure 15. Influence of cyclic pitch on bender tip displacement on bender tip motion: ——, $\theta = 0$; ------, $\theta = 1$; – – –, $\theta = 2$; — —, $\theta = 3$.

twist and bender tip motion. The conclusions drawn from this result is that the bender has some slight influence on the blade twist deflection but the bender excited motion cannot be influenced by applying voltage to piezoelectric elements.

The influence of advance ratio and bender radial position on the blade/bender motion is investigated next. The amplitudes of blade twist angles and bender tip deflections are shown in Figure 14 as functions of bender radial placement for different advance ratios. For constant advance ratio, blade twist amplitude does not depend on bender placement. The bender tip amplitude increases rapidly with radial distance from the shaft axis but

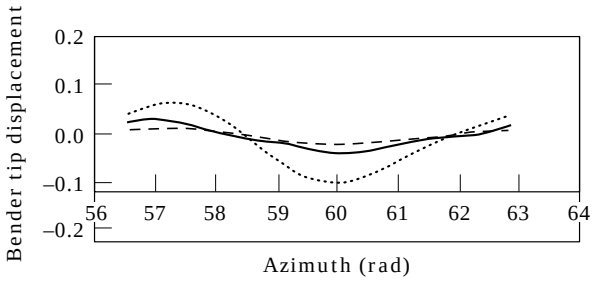

Figure 16. Influence of beam and layers thickness: ------, $h_b = 0{\cdot}005$, $h_l = 0{\cdot}0005$; ——, $h_b = 0{\cdot}0075$, $h_l = 0{\cdot}001$; – – –, $h_b = 0{\cdot}01$, $h_l = 0{\cdot}001$.

stabilises outboard of $0{\cdot}25R$. It can be concluded that there is a very narrow margin of blade placement radius and advance ratio within which the bender tip deflections are acceptable.

The next case, Figure 15, illustrates the influence of cyclic pitch on bender motion for the bender placed close to the blade root at $r = 0{\cdot}13R$ and for zero advance ratio. The blade collective pitch is 13° and the longitudinal and lateral cyclic pitch angles are varied. Two cases are compared, namely, bender free and excited at 1 per rev and 200 V. The cyclic pitch excitation enables the bender motion to be influenced for the design parameters chosen.

Some results of a parametric study undertaken to investigate the influence of the beam/bender thickness ratio on the possibility of influencing the device motion are presented in Figure 16. For all cases it was impossible to stabilise bender motion, even when applying a higher voltage of 600 V.

5. CONCLUSIONS

From the current study it can be concluded, that: (1) The concept of suppressing vibrations by applying only dynamic loads along part of the blade span can lead to substantial vibration reduction in terms of blade root loads. (2) Suppressing one load component can lead to suppression of the others. This result may be useful both for vibration suppression concept and control system design. (3) A practically configured bender type device mounted inside a realistic blade is subjected to considerable excitation due to blade motion. Attempts to reduce this excited motion by applying even very thick PZT layers and exciting them by high voltage transpired to be unsuccessful. (4) Blade cyclic pitch can be regarded as the main factor causing excessive bender movement. The results have implications for the use of bender type devices in operating blade mounted tabs.

ACKNOWLEDGMENT

The present work forms a part of a research programme funded by UK EPSRC on "Application of Smart Structures to Helicopter Rotor Blade Design".

REFERENCES

1. J. Narkiewicz and G. T. S. Done 1994 *Second European Conference on Smart Structures and Materials*. An overview of smart structure concepts for helicopter rotor control.
2. H. Strelhow and H. Rapp 1992 *AGARD/SMP Specialist's Meeting on Smart Structures for Aircraft and Spacecraft*. Smart materials for helicopter rotor active control.
3. F. K. Straub 1993 49*th American Helicopter Society Forum*. A feasibility study of using smart materials for rotor control.
4. I. Chopra 1993 *XIX European Rotorcraft Forum*. Development of smart rotor.
5. Y. K. Yillikci 1992 *XIX European Rotorcraft Forum*. Aeroelastic analysis of rotor blades with flap control.
6. T. A. Millot and P. P. Friedmann 1993 49*th American Helicopter Society Forum*. The practical implementation of an actively controlled flap to reduce vibrations in helicopter rotors.
7. F. K. Straub, L. H. Robinson 1993 49*th American Helicopter Society Forum*. Dynamics of a rotor with nonharmonic control.
8. J. Narkiewicz and M. Rogusz 1993 *XIX European Rotorcraft Forum*. Smart flap for helicopter rotor blade performance improvement.
9. J. Narkiewicz 1994 *Scientific Report*, *Series Mechanics* **158**. Publishing House of Warsaw University of Technology. Rotorcraft aeromechanical and aeroelastic stability (in Polish).

10. J. C. Houbolt and G. W. Brooks 1957 *NACA Rep*. 1346. Differential equations of motion for combined flapwise bending, chordwise bending and torsion of twisted nonuniform rotor blades.
11. A. R. S. Bramwell 1976 *Helicopter Dynamics*, London: Edward Arnold.
12. T. Kreglewski, T. Rogowski, A. Ruszczynski and J. Szymanowski 1984 *Optimization Methods in FORTRAN* (in Polish).
13. B. H. Lau, A. W. Louie, N. Griffiths and C. P. Sotiriou 1993 *NASA TM* 104000. Performance and rotor loads measurements on the Lynx XZ170 helicopter with rectangular blades.
14. T. Meressi and B. Paden 1993 *Journal of Guidance, Control and Dynamics* **16**, 859–864. Piezoelectric actuator design for vibration suppression: placement and sizing.

APPENDIX A

The elements of matrices **B** and **C** and vectors $\mathbf{f}_m$ and $\mathbf{g}_m$ are given below

$$B_{ni} = \int_R \int_A \rho_b \left(\frac{\partial \mathbf{r}_0}{\partial q_n}\right)^T \left(\frac{\partial \mathbf{r}_0}{\partial q_i}\right) \mathrm{d}A \ \mathrm{d}R, \qquad C_{ni} = \int_R \int_A \rho_b \left(\frac{\partial \mathbf{r}_0}{\partial q_n}\right)^T \mathbf{D}^T \dot{\mathbf{D}} \left(\frac{\partial \mathbf{r}_0}{\partial q_i}\right) \mathrm{d}A \ \mathrm{d}R,$$

$$f_{mn} = \int_R \int_A \rho_b \left(\frac{\partial \mathbf{r}_0}{\partial q_n}\right)^T \mathbf{D}^T \dot{\mathbf{D}} \mathbf{r}_0 \ \mathrm{d}A \ \mathrm{d}R,$$

$$g_{mn} = \sum_{i=1}^{N_g} \sum_{j=1}^{N_g} \dot{q}_i \dot{q}_j \int_R \int_A \rho_b \left(\frac{\partial \mathbf{r}_0}{\partial q_n}\right)^T \left(\frac{\partial^2 \mathbf{r}_0}{\partial q_i \partial q_j}\right) \mathrm{d}A \ \mathrm{d}R,$$

where **D** is the transformation matrix due to shaft rotation, ρ_b is the blade density, $\mathbf{r}_0$ is the position vector of the blade point, A is the blade cross-section, R is the blade length and q_i are the generalised co-ordinaters of the blade motion.

APPENDIX B

Matrix **A**

$$a_{ii} = \int_R \int_A \{[EI \cos^2(\theta_g) + EJ \sin^2(\theta_g)](\eta_i'')^2 + t_s(x)(\eta_i')^2\} \ \mathrm{d}A \ \mathrm{d}R, \qquad i = 1, \ldots, N_v,$$

$$a_{ij} = -\int_R \int_A \{[EI - EJ] \cos(\theta_g) \sin(\theta_g) \eta_i'' \eta_j''\} \ \mathrm{d}A \ \mathrm{d}R, \qquad i = 1, \ldots, N_{v,},$$

$$j = N_w + 1, \ldots, N_w,$$

$$a_{ij} = \int_R \int_A \{(\theta_g') C_\eta \cos(\theta_g) \eta_i' \eta_j'' + t_s(x) \eta_s \sin(\theta_g) \eta_i'' \eta_j\} \ \mathrm{d}A \ \mathrm{d}R, \qquad i = 1, \ldots, N_v,$$

$$j = N_w + N_w + 1, \ldots, Nw_+ N_w + N_f,$$

$$a_{ii} = \int_R \int_A \{[EI \sin^2(\theta_g) + EJ \cos^2(\theta_g)](\eta_i'')^2 + t_s(x)(\eta_i')^2\} \ \mathrm{d}A \ \mathrm{d}R,$$

$$i = N_v + 1, \ldots, N_w + N_w,$$

$$a_{ij} = \int_R \int_A \{(\theta_g')C_\eta \sin(\theta_g)\eta_i'\eta_j'' + t_s(x)\eta_s \cos(\theta_g)\eta_i''\eta_j\}\, \mathrm{d}A\, \mathrm{d}R,$$

$$i = N_v + 1, \ldots, N_w + N_w \quad j = N_w + N_w + 1, \ldots, N_w + N_w + N_f,$$

$$a_{ij} = \int_R \int_A \{[GJ + (\theta_g')L_K + t_s(x)K_E\eta_s](\eta_j')^2\}\, \mathrm{d}A\, \mathrm{d}R,$$

$$i = N_w + N_w + 1, \ldots, Nw_+ N_w + N_f.$$

Vector **h**

$$h_1 = -\int_R \int_A \{t_s(x)\eta_s \cos(\theta_g)\eta_i''\}\, \mathrm{d}A\, \mathrm{d}R, \qquad i = 1, \ldots, N_w,$$

$$h_1 = \int_R \int_A \{t_s(x)\eta_s \sin(\theta_g)\eta_j''\}\, \mathrm{d}R\, \mathrm{d}A, \qquad i = N_w + 1, \ldots, N_w + N_w,$$

$$h_1 = \int_R \int_A \{t_s(x)K_E\theta_g'\eta_j'\}\, \mathrm{d}A\, \mathrm{d}R, \qquad i = N_w + N_w + 1, \ldots, N_{w+}N_w + N_f$$

where

$$t_s = \int_R \int_A [\rho_b(\Omega z)^2]\, \mathrm{d}A\, \mathrm{d}z, \qquad A_E = \int_A E\, \mathrm{d}A, \qquad \eta_s = \frac{1}{A_E}\int_A E\eta\, \mathrm{d}A,$$

$$k_T = \frac{1}{A_E}\int_A E(\eta^2 + \varsigma^2)\, \mathrm{d}A,$$

$$K_E = \frac{1}{A_E}\int_A E(\eta^2 + \varsigma^2 - k_T)\, \mathrm{d}A, \qquad L_K = \int_A E(\eta^2 + \varsigma^2 - k_T)^2\, \mathrm{d}A,$$

$$C_\eta = \int_A E(\eta^2 + \varsigma^2 - k_T)(\eta - \eta_s)\, \mathrm{d}A,$$

$$GJ = \int_A G(\eta^2 + \varsigma^2)\, \mathrm{d}A, \qquad EJ = \int_A E\varsigma^2\, \mathrm{d}A, \qquad EI = \int_A E(\eta - \eta_s)^2\, \mathrm{d}A.$$